

Article

Optimizing the Aromatic Product Distribution from Catalytic Fast Pyrolysis of Biomass Using Hydrothermally Synthesized Ga-MFI Zeolites

Jian Li ^{1,2}, Xiangyu Li ³, Derun Hua ¹, Xinning Lu ¹ and Yujue Wang ^{2,*}

¹ College of Chemistry and Chemical Engineering, Gannan Normal University, Ganzhou 341000, China; lijian@sxicc.ac.cn (J.L.); dr_hua2011@sina.com (D.H.); luxinning@gnnu.edu.cn (X.L.)

² School of Environment, State Key Joint Laboratory of Environmental Simulation and Pollution Control, Tsinghua University, Beijing 100084, China

³ China National Tobacco Quality Supervision and Test Center, No. 2 Fengyang street, Zhengzhou 450001, China; lixiangyu_10@163.com

* Correspondence: wangyujue@tsinghua.edu.cn; Tel.: +86-10-6277-2914; Fax: +86-10-6278-5687

Received: 22 September 2019; Accepted: 9 October 2019; Published: 13 October 2019



Abstract: A series of gallium-containing MFI (Ga-MFI) zeolites with varying Ga₂O₃/Al₂O₃ ratios were synthesized using hydrothermal synthesis and tested as catalyst in catalytic fast pyrolysis (CFP) of beech wood for aromatic production. The results show that the incorporation of Ga slightly reduced the effective pore size of Ga-MFI zeolites compared to conventional HZSM-5 zeolites. Therefore, the Ga-MFI zeolites increased the aromatic selectivity for smaller aromatics such as benzene, toluene, and *p*-xylene and decreased the aromatic selectivity for bulkier ones such as *m*-xylene, *o*-xylene, and polyaromatics in CFP of beech wood relative to HZSM-5. In particular, the yield and selectivity of *p*-xylene, the most desired product from CFP of biomass, increased considerably from 1.64 C% and 33.3% for conventional HZSM-5 to 2.98–3.34 C% and 72.1–79.6% for the synthesized Ga-MFI zeolites. These results suggest that slightly reducing the pore size of MFI zeolite by Ga incorporation has a beneficial effect on optimizing the aromatic selectivity toward more valuable monoaromatic products, especially *p*-xylene, during CFP of biomass.

Keywords: aromatics; biomass; MFI zeolites; gallium; catalytic fast pyrolysis

1. Introduction

Aromatic hydrocarbons derived from petroleum are widely used to manufacture a wide range of downstream products, such as synthetic plastic, medicine, and gasoline additives. As the petroleum reserves around the world are depleting at a fast rate, producing renewable aromatics from lignocellulosic biomass has gained increasing interest [1,2]. Lignocellulosic biomass is the most abundant and sustainable carbon resource on the earth [3]. It has therefore been considered attractive feedstock for producing valuable aromatic hydrocarbons, such as benzene, toluene, and xylenes (BTXs), which are the building-blocks of the petrochemical industry to produce numerous petrochemical intermediates and commercial products [1,4,5]. Among many conversion technologies, catalytic fast pyrolysis (CFP) of biomass with zeolite catalysts has attracted growing attention because it can directly convert lignocellulosic biomass to valuable aromatic hydrocarbons, especially BTXs.

During CFP of biomass, the framework and acidity of zeolite catalysts play an important role in the distribution of final products [6–9]. Among many zeolites that have been tested, ZSM-5 zeolite has been shown to produce high aromatic yields from biomass-derived feedstocks [8,10,11]. The high aromatic yields of HZSM-5 can be primarily attributed to its moderate acid sites and suitable micropore size,

which have a beneficial effect on the acid sites-catalyzed reactions of biomass to aromatic hydrocarbons (e.g., deoxygenation, oligomerization, and aromatization) [8,12].

Although ZSM-5 zeolite can produce higher aromatic yields compared with other zeolites, polyaromatics usually contain significant fractions (~30–40%) of the final aromatics in CFP of biomass [13–15]. Because of their low value and high mutagenicity, polyaromatics are usually considered undesired products from CFP of biomass [16]. Moreover, ZSM-5 zeolite exhibits low selectivity (~30–53%) for *p*-xylene, which is the most desirable aromatic product from CFP because of its high value and importance for polyethylene terephthalate production [17]. These results indicate that the product distribution from CFP of biomass with the conventional ZSM-5 zeolite still has vast potential for further improvement.

Impregnation or incorporation of ZSM-5 with gallium (Ga) has been shown to be able to reduce the selectivity for polyaromatics and favor the production of *p*-xylenes from CFP of biomass, thus improving the aromatic product distributions [16,17]. This improvement is mainly caused by the slight decrease of the pore size of ZSM-5 by Ga modification, which promotes the formation of smaller monoaromatics (e.g., benzene, toluene, and *p*-xylene) over bulkier ones (e.g., *m*-, and *o*-xylene and naphthalenes) [16]. In a previous study [16], we found that incorporating Ga into the framework of ZSM-5 by hydrothermal synthesis is more effective at improving the aromatic product distribution from CFP of biomass than impregnation of ZSM-5 with Ga. This difference has been attributed to the fact that impregnation can only result in Ga-oxides (e.g., Ga₂O₃ and GaO⁺) to disperse on the external surface of the zeolites [16]. In contrast, non-framework Ga-oxides can be formed both on the external surface and in the channels of zeolites, due to the degallation of framework Ga during calcination of the hydrothermal synthesized Ga-containing ZSM (GaMFI) to H-form zeolites [16].

Desilication of ZSM-5 zeolites with sodium hydroxide (NaOH) has also been considered a simple and effective way to improve the aromatic yield and distribution from CFP of biomass [18]. Due to the creation of mesopores in ZSM-5 by NaOH desilication, the catalytic activity and diffusion properties of the zeolites are improved, favoring the production of valuable monoaromatics over undesired polyaromatics relative to the conventional microporous ZSM-5 [19–21]. Further impregnation of desilicated HZSM-5 with gallium can promote dehydrogenation and aromatization in methanol to gasoline process [22]. Because Ga-containing MFI zeolite via hydrothermal synthesis produced more valuable monoaromatics than conventional HZSM-5 zeolite impregnated with gallium, we anticipated that direct desilication of Ga-containing MFI zeolite may provide an effective way to enhance biomass conversion and optimize product distribution in CFP.

To test this hypothesis, we synthesized a series of Ga-containing MFI zeolites with different Ga₂O₃/Al₂O₃ ratios. Mesoporous Ga-containing MFI zeolite was then prepared by desilication of a microporous Ga-containing MFI zeolite with NaOH solutions. The effects of gallium incorporation and NaOH desilication on the structural properties and acidity of MFI zeolites were examined using various methods. CFP of beech wood with HZSM-5 and Ga-containing MFI zeolites were compared to investigate the effects of gallium incorporation on the monoaromatic hydrocarbons distribution in this research.

2. Results and Discussion

2.1. Zeolite Characterizations

The chemical and framework properties of HZSM-5 and the Ga-containing MFI zeolites are summarized in Table 1. The Ga₂O₃/Al₂O₃ ratio of GaMFI zeolites increased from 1.2 to 2.3 with increasing the ratio of precursor solutions during the preparation. Additionally, it is noticed that DS-GaMFI2 zeolite had the same Ga₂O₃/Al₂O₃ ratio of 1.7 as GaMFI2, indicating that alkaline treatment does not considerably remove Ga or Al from the zeolite structure [23–25].

Table 1. Characterizations of the HZSM-5 and Ga-containing MFI zeolites.

Catalyst	Ga ₂ O ₃ ^a (%)	Ga ₂ O ₃ /Al ₂ O ₃ ^a	SiO ₂ /(Al ₂ O ₃ + Ga ₂ O ₃) ^a	S _{BET} ^b (m ² /g)	V _{total} ^c (cm ³ /g)	V _{micro} ^c (cm ³ /g)	V _{meso} ^d (cm ³ /g)	A _{Brönsted} ^e (μmol/g)	A _{Lewis} ^e (μmol/g)
HZSM-5	-	-	25.5	423.7	0.211	0.158	0.053	340.2	75.6
GaMFI1	4.72	1.2	33.0	412.0	0.233	0.165	0.068	198.5	85.3
GaMFI2	5.09	1.7	36.0	394.3	0.204	0.148	0.056	201.4	76.8
GaMFI3	5.56	2.3	36.6	407.5	0.229	0.164	0.065	160.4	85.2
DS-GaMFI2	5.74	1.7	31.5	404.0	0.254	0.139	0.115	129.5	95.2

^a By XRF analysis. ^b From N₂ adsorption measurements (BET method). ^c From N₂ adsorption measurements (*t*-plot).

^d From N₂ adsorption measurements (BJH method). ^e Measured by IR spectroscopy of absorbed pyridine at 200 °C.

Nitrogen adsorption/desorption results show that the GaMFI zeolites (GaMFI1, GaMFI2, and GaMFI3) had lower BET surface area (394.3–412.0 m²/g) than HZSM-5 (423.7 m²/g). Similar results have been reported in previous studies and attributed to the occupation of a part of channel space by the non-framework Ga-oxides formed during degalliation [26,27]. For the DS-GaMFI2 zeolite, its mesopore volume increased to 0.115 cm³/g compared with GaMFI2 (0.056 cm³/g). In contrast to its mesoporosity, the micropore volume dropped from 0.148 cm³/g for GaMFI2 to 0.139 cm³/g for DS-GaMFI2 after alkaline treatment (see Table 1). This is because the fraction of mesoporosity increased at the expense of microporosity during alkaline treatment of GaMFI2, agreeing with previous works [18,28,29].

Acidity quantification by pyridine adsorption exhibits that the density of Brönsted acidity decreased significantly for GaMFI zeolites, while the Lewis acidity increased compared with HZSM-5. This decrease is partly attributed to the replacement of some Brönsted acid sites by gallium [30,31]. Additionally, the previous findings have revealed that Brönsted acid sites are mostly ascribed to bridged silanol groups (Si–OH–Al) and gallium species (Si–OH–Ga), and Si–OH–Ga sites are more covalent than Si–OH–Al. Therefore, GaMFI zeolites have lower Brönsted acidity than HZSM-5. In contrast, Lewis acid sites are generally associated with non-framework Al and Ga species [26,27]. Because non-framework gallium oxides generated during calcination of GaMFI contribute to Lewis acid sites [27,32], GaMFI zeolites had higher Lewis acidity than HZSM-5. In addition, the acidity of GaMFI2 was changed significantly by alkaline treatment. Compared with GaMFI2, DS-GaMFI2 had much less Brönsted acidity and more Lewis acidity, suggesting that partial Brönsted acid sites were transformed to Lewis acid sites during the alkaline treatment. This is mainly because, while internal silanol sites are removed upon desilication, extracted Al are precipitated on the exterior surface of the zeolite [33,34].

XRD analysis results show that all samples exhibited the characteristic peaks of the MFI-type zeolite at ~8° and 23° (see Figure 1). This result suggests that the framework of the GaMFI zeolites is the same as that of HZSM-5 zeolite. No crystalline phases of bulk Ga-oxides are detected in the XRD profiles of GaMFI zeolites, suggesting that non-framework Ga-oxides were highly dispersed on external surfaces or the channel of the zeolites [30,35]. In addition, a closer examination of the peak at ~23° exhibits that the relative crystallinity of DS-GaMFI2 was nearly the same (96%) as the parent GaMFI2 zeolite. This result is generally in line with previous findings that desilication of ZSM-5 with 0.2 M NaOH solution does not affect the crystallinity of desilicated zeolite [23].

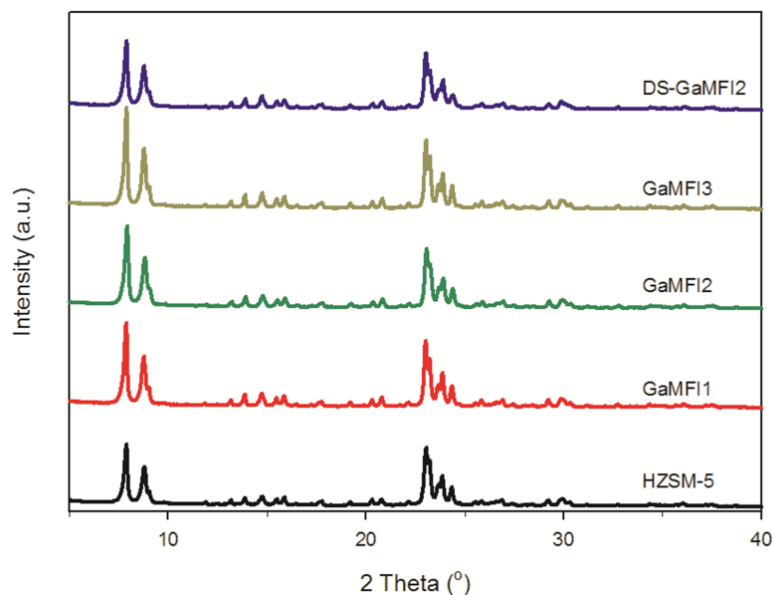


Figure 1. XRD patterns of HZSM-5 and Ga-containing MFI zeolites.

The existing forms of non-framework Ga-oxides were measured with H_2 -TPR analyses. As shown in Figure 2, the GaMFI zeolites exhibit two major hydrogen reduction peaks, which are ascribed to the reduction of non-framework Ga species, since the framework Ga species cannot be reduced in the range of 200 to 900 °C [27,35]. The two significant hydrogen consumption peaks at ~400 °C and ~530 °C can be assigned to the reduction of highly dispersed Ga_2O_3 and GaO^+ , respectively [35–37]. For GaMFI zeolites, the second peak is more pronounced than the first one, indicating that their non-framework Ga-oxides are mostly present as GaO^+ . In contrast, DS-GaMFI2 zeolite had a much weaker reduction peak of GaO^+ . This is probably because non-framework GaO^+ is partially extracted during the desilication of GaMFI2 with alkaline solution.

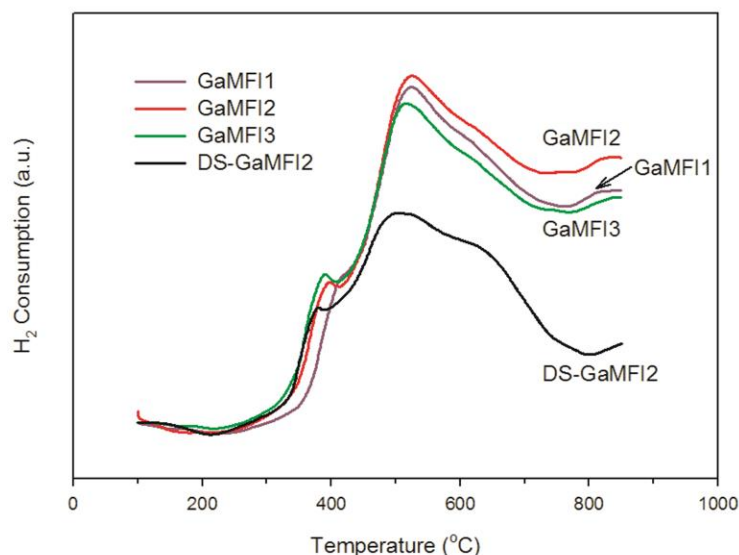


Figure 2. H_2 -TPR profiles of Ga-containing MFI zeolites.

The overall results presented above indicate that non-framework Ga-oxides changed the porosity and acidity of Ga-containing zeolites (the synthesized GaMFI zeolites) considerably. In addition, alkaline treatment also had a significant influence on the structural and chemical catalytic properties of

desilicated GaMFI zeolites. These changes in turn influenced the CFP product distribution, which are evaluated in the following section.

2.2. CFP of Beech Wood with HZSM-5 and the Ga-Containing MFI Zeolites

CFP of beech wood with the conventional HZSM-5 and GaMFI zeolites produced similar final products, including mainly monoaromatics (benzene, toluene, xylene, alkylbenzene, and indene), polyaromatics (naphthalene, methylnaphthalene, and dimethylnaphthalene), $\leq C_5$ olefins and alkanes, carbon oxides, and solid residue (char and coke) (see Table 2 for detailed yields of the products). However, the product distribution was changed to different extents due to ZSM-5 modification with Ga incorporation and NaOH desilication.

Table 2. Product distribution in CFP of beech wood with HZSM-5 and Ga-containing MFI zeolites.

Carbon Yield (C%)	HZSM-5	GaMFI1	GaMFI2	GaMFI3	DS-GaMFI2
Aromatic hydrocarbons					
Benzene	1.96 ± 0.01	2.40 ± 0.03	1.72 ± 0.01	1.81 ± 0.13	1.92 ± 0.14
Toluene	4.91 ± 0.06	6.28 ± 0.03	4.56 ± 0.01	4.77 ± 0.36	4.55 ± 0.35
Ethylbenzene	0.15 ± 0.01	0.35 ± 0.00	0.27 ± 0.00	0.32 ± 0.02	0.38 ± 0.02
<i>p</i> -Xylene	1.64 ± 0.06	3.34 ± 0.05	2.79 ± 0.01	2.98 ± 0.12	2.20 ± 0.15
<i>m</i> -Xylene	2.43 ± 0.05	1.05 ± 0.09	0.62 ± 0.02	0.64 ± 0.08	2.42 ± 0.20
<i>o</i> -Xylene	0.85 ± 0.00	0.24 ± 0.00	0.14 ± 0.01	0.13 ± 0.02	0.86 ± 0.08
1,2,4-Trimethylbenzene	0.47 ± 0.01	0.10 ± 0.01	0.07 ± 0.00	0.07 ± 0.01	0.78 ± 0.06
Indane	0.21 ± 0.01	0.24 ± 0.01	0.17 ± 0.00	0.20 ± 0.01	0.31 ± 0.02
Indene	0.16 ± 0.01	0.27 ± 0.00	0.20 ± 0.00	0.23 ± 0.01	0.28 ± 0.02
Naphthalene	1.53 ± 0.01	1.65 ± 0.05	1.05 ± 0.02	1.14 ± 0.11	0.69 ± 0.06
1-methylnaphthalene	0.13 ± 0.01	0.01 ± 0.00	0.00 ± 0.00	0.01 ± 0.00	0.06 ± 0.00
2-methylnaphthalene	1.82 ± 0.05	1.15 ± 0.05	0.63 ± 0.01	0.85 ± 0.06	0.66 ± 0.05
2,7-dimethylnaphthalene	1.17 ± 0.05	0.47 ± 0.03	0.26 ± 0.00	0.35 ± 0.02	0.52 ± 0.04
Olefins					
Ethylene	2.25 ± 0.08	2.13 ± 0.05	2.14 ± 0.05	1.99 ± 0.05	2.22 ± 0.10
Propene	1.00 ± 0.04	1.14 ± 0.03	1.25 ± 0.01	1.19 ± 0.08	1.46 ± 0.08
C ₄ olefins	0.31 ± 0.02	0.36 ± 0.01	0.38 ± 0.00	0.42 ± 0.01	0.45 ± 0.02
C ₅ olefins	0.09 ± 0.00	0.12 ± 0.01	0.12 ± 0.01	0.14 ± 0.02	0.16 ± 0.02
Alkanes					
Methane	0.64 ± 0.02	0.74 ± 0.01	0.73 ± 0.02	0.70 ± 0.04	0.63 ± 0.01
Ethane	0.24 ± 0.01	0.12 ± 0.00	0.10 ± 0.01	0.10 ± 0.02	0.09 ± 0.00
Propane	1.15 ± 0.04	0.48 ± 0.02	0.37 ± 0.02	0.36 ± 0.04	0.35 ± 0.02
C ₄ alkanes	0.19 ± 0.01	0.11 ± 0.00	0.09 ± 0.01	0.10 ± 0.01	0.11 ± 0.01
C ₅ alkanes	0.03 ± 0.00	0.02 ± 0.00	0.02 ± 0.00	0.02 ± 0.00	0.03 ± 0.00
CO and CO ₂	24.28 ± 1.45	24.20 ± 3.55	20.73 ± 0.24	19.55 ± 0.46	20.47 ± 0.03
Char/Coke	50.2 ± 0.71	46.5 ± 0.58	47.0 ± 0.55	45.5 ± 0.21	50.9 ± 0.56

Figure 3 shows carbon yields of the final products from CFP of beech wood with HZSM-5 and Ga-containing MFI zeolites. When HZSM-5 zeolites were used as the catalyst, the condensable products consisted of mostly monoaromatics (12.7 C%) and polyaromatics (4.6 C%). In comparison, the GaMFI zeolites (GaMFI1, GaMFI2, and GaMFI3) produced fewer amounts of polyaromatics (1.9–3.2 C%). In addition, the GaMFI zeolites also produced less char/coke (45.5–47.0 C%) than the conventional HZSM-5 (50.2 C%). These observations confirm that incorporation of non-framework Ga-oxides into MFI zeolites can considerably change the distribution of final products.

The formation of aromatic hydrocarbons from CFP of biomass generally includes two steps: (1) Thermal decomposition of the biomass to small oxygenates, and (2) catalytic conversion of these oxygenates to final products (aromatic hydrocarbons, gaseous hydrocarbons, char/coke, and CO&CO₂) via a series of acid sites-catalyzed reactions, involving deoxygenation, oligomerization, aromatization, and dealkylation [38–40]. During the conversion process, the catalytic reactions occur primarily inside the micropores of zeolites, which are about the same size of the critical diameter of polyaromatic hydrocarbons (e.g., 2-methylnaphthalene, 7.752 Å). Compared with HZSM-5, GaMFI zeolites produced

lower yields of polyaromatic hydrocarbons (Figure 3), indicating that the formation of these bulky hydrocarbons was inhibited due to the decrease of micropore size of ZSM-5 by Ga modification. This observation is consistent with the previous findings [30,31] that GaMFI zeolites had a narrowed micropore because partial micropore spaces were occupied by the non-framework Ga-oxides formed during zeolite calcinations.

It is noticed that DS-GaMFI2 had a much higher monoaromatic hydrocarbon yield (13.7 C%) than GaMFI2 (10.5 C%). This improvement suggests that the desilicated GaMFI zeolite can convert the biomass-derived oxygenates to monoaromatics more effectively than GaMFI2. This improvement can be attributed to the fact that alkaline treatment can create mesopores in zeolites, which shortens the micropore diffusion length [18,41]. As a result, monoaromatic hydrocarbons can diffuse out of the mesopores of DS-GaMFI2 rather than being absorbed by acid sites to form polyaromatics via alkylation reaction [18,19,42].

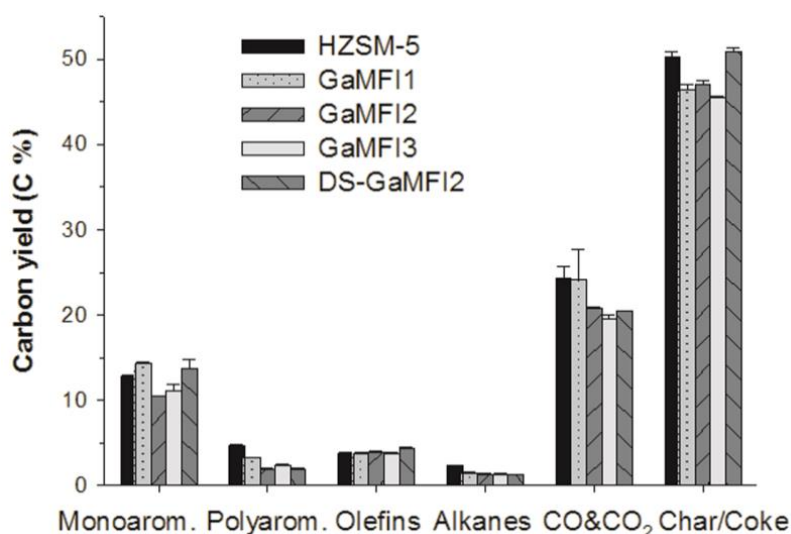


Figure 3. Carbon yields of major products in CFP of beech wood with HZSM-5 and Ga-containing MFI zeolites.

Figure 4 shows the selectivity of major aromatics from CFP of beech wood with HZSM-5 and Ga-containing MFI zeolites. Compared to HZSM-5, GaMFI incorporation considerably increased the selectivity for the valuable monoaromatic hydrocarbons (e.g., BTXs) during CFP of beechwood. As discussed previously, this improvement can be mainly ascribed to the narrowed micropore channel of GaMFI zeolites, which facilitates the production of smaller monoaromatics over bulkier polyaromatics via the shape selective mechanism [32,43]. However, subsequent desilication of GaMFI2 zeolite with alkaline treatment (DS-GaMFI2) did not considerably further enhance BTX selectivity compared to GaMFI2 (77.0% vs. 79.1%). Specifically, while the selectivity for xylenes increased from 28.6% for GaMFI2 to 35.2% for DS-GaMFI2, the selectivity for toluene decreased substantially from 36.7% to 29.2%. The inverse dynamics of toluene and xylene selectivity indicate that the creation of mesoporous in DS-GaMFI2 had a complex influence on the monoaromatic distribution in CFP of biomass.

Interestingly, the change of $\text{Ga}_2\text{O}_3/\text{Al}_2\text{O}_3$ ratio for GaMFI zeolites during hydrothermal synthesis had no pronounced effects on the aromatic selectivity (Figure 4a), but changed the xylene selectivity and *p*-xylene yield considerably (see Figure 4b). The selectivity and yield for *p*-xylene, the most desired xylene from CFP of biomass, increased from 33.3% and 1.64 C% for HZSM-5 to 72.1–79.6% and 2.79–3.34 C% for GaMFI zeolites, respectively. It is well-known that the aromatic product distribution in CFP of biomass is strongly affected by the porosity of zeolites [11,44]. Because the effective pore size of ZSM-5 at the high temperatures of CFP (e.g., ~ 8.1 Å at 650 °C) is slightly larger than the critical diameter of *p*-xylene ($d_c = \sim 6.7$ Å) [11], conventional HZSM-5 zeolite does not favor the formation of *p*-xylene, but favors the formation of bulkier *m*-xylene ($d_c = 7.4$ Å). Note that the critical diameter of a

molecule is conventionally defined as the diameter of the smallest cylinder that can circumscribe the molecule in its most favorable equilibrium conformation [44] and can be calculated using quantum chemical computations [11,16]. In contrast, due to the slight narrowing of the pore diameter of ZSM-5 by Ga incorporation, GaMFI zeolites enhanced both the selectivity and yield for *p*-xylene considerably, thus improving the product distribution in CFP of biomass towards more valuable product.

Compared with Ga impregnation, which is a more conventional way to modify ZSM-5 for *p*-xylene production [31,45], hydrothermal synthesis of GaMFI appears to be a more effective option to enhance the *p*-xylene during CFP of biomass. For instance, Cheng et al. [46] reported that impregnation of ZSM-5 with gallium (Ga/HZSM-5) increased *p*-xylene selectivity only marginally from 53% for conventional HZSM-5 to 58% for Ga/HZSM-5 in CFP of furan and did not increase *p*-xylene yield. In comparison, this present study shows that hydrothermally synthesized GaMFI zeolites considerably increased both the yield and selectivity for *p*-xylene. This improvement can possibly be attributed to the different mechanisms of pore narrowing by Ga impregnation and by Ga incorporation. Ga impregnation reduces the effective pore size of ZSM-5 by partially blocking the pore opening of zeolites with Ga-oxides, whereas Ga incorporation reduces the pore size of zeolites mainly by depositing non-framework Ga-oxides inside the zeolite channels during calcination [16]. It is noticed that the selectivity for *p*-xylene increased to 72.1, 78.5, and 79.6% for the three GaMFI zeolites with the increase of the Ga₂O₃/Al₂O₃ ratio. This trend suggests that increasing the Ga₂O₃/Al₂O₃ ratio resulted in more effective pore size reduction of the GaMFI, and thus increased the selectivity for *p*-xylene during CFP [26,32].

In contrast to GaMFI2 zeolite, DS-GaMFI2 zeolite produced lower yield and selectivity of 2.20 C% and 44.1% for *p*-xylene (see Figure 4b). This decrease can possibly be attributed to the fact that the microporosity of GaMFI2 is reduced during desilication by alkaline treatment [42,47], which decreases the isomerization of *m*- and *o*-xylenes to *p*-xylene inside the zeolite micropores.

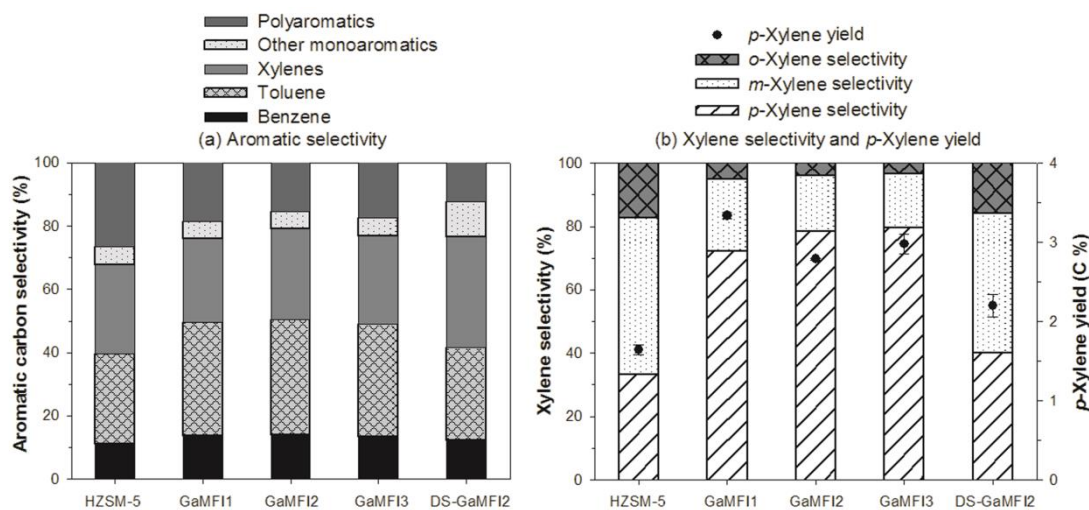


Figure 4. (a) Aromatic products selectivity, and (b) xylene selectivity and *p*-xylene yields from CFP of beech wood with HZSM-5 and Ga-containing MFI zeolites.

To further illustrate the change of aromatic product distribution due to Ga incorporation and NaOH desilication, we compared the yield of each aromatic product from CFP of beech wood with GaMFI zeolites (GaMFI1, GaMFI2, and GaMFI3) to that with HZSM-5 zeolite. This ratio shows whether the production of a given aromatic is inhibited (if the ratio is <1) or promoted (if the ratio is >1) when HZSM-5 is replaced with the GaMFI zeolites. The ratio for each aromatic is then plotted against its critical diameter (d_c) (see Figure 5). As shown in Figure 5a–c, the ratio is considerably higher than 1 for *p*-xylene, indicating that its yield was significantly enhanced when GaMFI zeolites were used in CFP of beech wood. In contrast, the ratios are lower than 1 for aromatics with $d_c > 7.3$ Å (i.e., *m/o*-xylene, 1,2,4-trimbenzene, methylnaphthalenes, and 2,7-dimethylnaphthalene), indicating that

their production was suppressed. Overall, a general trend can be observed in the figures, that the ratio between the aromatic yield for GaMFI and HZSM-5 zeolites decreases with increasing the diameter of aromatic products. This trend suggests that the production of bulkier aromatics is inhibited when GaMFI zeolites were used in CFP of beech wood.

In addition, we compared the aromatic yield of the desilicated GaMFI2 zeolite (DS-GaMFI2) to that of GaMFI2 for each product (see Figure 5d). The results show that the ratios are generally >1 for aromatic products (with the exception of *p*-xylene), indicating that their yields were enhanced when GaMFI2 was desilicated by alkaline treatment. Notably, the ratios for the larger aromatic hydrocarbons with $d_c > 7.8 \text{ \AA}$ (e.g., 1,2,4-trimethylbenzene and 1-methylnaphthalene) are considerably higher than 1. This is probably because desilication creates intraparticle mesopores in zeolites, which shortens the micropore path length and facilitates the diffusion of these bulky aromatics [18,41]. As a result, 1,2,4-trimethylbenzene and 1-methylnaphthalene can diffuse out of the micropores of DS-GaMFI2 zeolite more easily to form the final aromatic products.

For xylene products, Figure 5d shows that the ratio for *p*-xylene ($d_c = 6.701 \text{ \AA}$) is lower than 1, whereas the ratios are remarkably higher than 1 for *m*-xylene ($d_c = 7.437 \text{ \AA}$) and *o*-xylene ($d_c = 7.345 \text{ \AA}$). These results indicate that DS-GaMFI2 zeolite significantly increased the production of meta and ortho xylenes over its para isomers relative to GaMFI2 zeolite. This change can be mainly attributed to the fact that desilication by alkaline treatment can enlarge the micropore size of DS-GaMFI2 zeolite slightly [42,48] and create some mesopores in the zeolites, which facilitate the diffusion of *m*-xylene and *o*-xylene. Therefore, desilication of GaMFI2 zeolite by alkaline treatment resulted in a negative effect on *p*-xylene production.

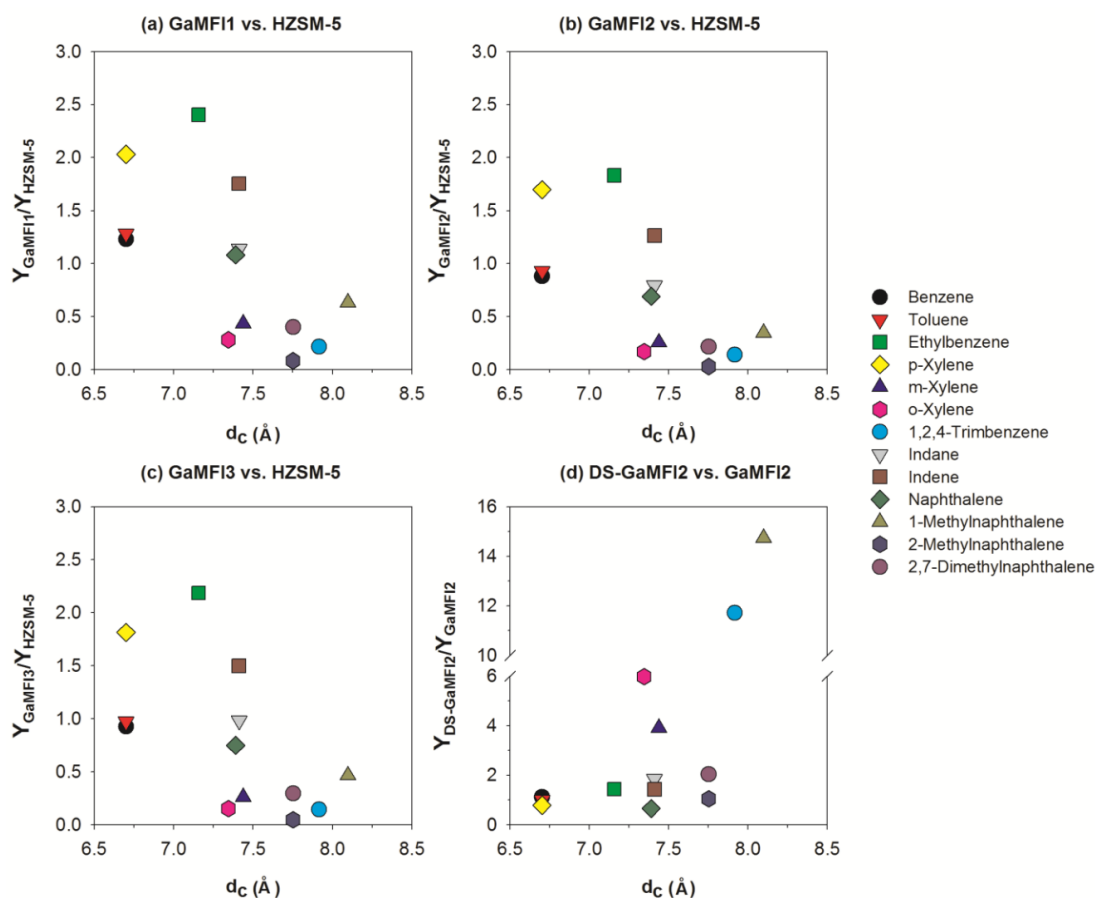


Figure 5. The ratio between the yield of aromatics in CFP of beech wood with HZSM-5 and Ga-containing MFI zeolites as a function of the molecular size of the aromatics. (a) GaMFI1 vs. HZSM-5; (b) GaMFI2 vs. HZSM-5; (c) GaMFI3 vs. HZSM-5; (d) DS-GaMFI2 vs. GaMFI2.

The above results show that hydrothermal synthesized GaMFI zeolites can effectively optimize aromatic hydrocarbons toward more valuable products (e.g., toluene and *p*-xylene) in CFP of biomass. This improvement can be mainly attributed to the decrease of the effective pore size of the zeolites due to the deposition of non-framework Ga-oxides in the micropores of GaMFI zeolites during calcination [16]. These narrowed micropores favor the production of relatively smaller aromatics (e.g., benzene, toluene, and *p*-xylene) over bulkier ones (e.g., *m*-xylene, trimethylbenzenes, and 1-methylnaphalene). Nevertheless, desilication of GaMFI2 zeolite with further alkaline treatment (DS-GaMFI2) resulted in lower yield and selectivity of *p*-xylene than GaMFI2. These comparisons suggest that desilicated GaMFI zeolites are not suitable catalysts for *p*-xylene production in CFP of lignocellulosic biomass because they have much more mesopores than GaMFI zeolites. Considering the fact that GaMFI zeolites exhibited highly selectivity for *p*-xylene, this report furnishes a new perspective for this subject, and provides new possibilities for desired petrochemical production from CFP of biomass.

3. Materials and Methods

3.1. Materials

Beech wood powder was purchased from a furniture factory in Beijing, and sieved through a 140 mesh (<0.105 mm) sieve. The elemental analysis of the beech wood was: C:H:N:O = 49.1:5.9:0.5:44.5. The microporous HZSM-5 zeolite (<0.105 mm) with a SiO₂/Al₂O₃ ratio of 25 was from the Catalyst Plant of Nankai University (Tianjin, China).

3.2. Zeolite Synthesis

The GaMFI zeolites were synthesized using the procedure described by Li et al. [16]. Silica gel (SiO₂, Aladdin), aluminum isopropoxide (Al₂O₃, Aladdin), Ga(NO₃)₃ (Ga₂O₃, Aladdin), tetrapropylammonium hydroxide (TPAOH, Aladdin), and deionized water were used as precursor solutions. The starting composition of synthesis gel was 25SiO₂:aGa₂O₃:bAl₂O₃:1Na₂O:5TPAOH:1500H₂O (a + b = 1, a/b = 1.2, 1.7, and 2.3). This gel mixture was transferred into a 200 mL autoclave and heated at ~190 °C for 72 h. After the completion of the synthesis, the crystalline product was washed repetitively with deionized water, dried overnight at 120 °C, and then calcined static air at 555 °C for 6 h. Finally, the GaMFI zeolites were transformed to acid form zeolites by ion exchange with 1.0 M NH₄NO₃ under reflux for 3 h, followed by drying and calcination. These hydrothermal synthesized GaMFI zeolites were donated as GaMFI1, GaMFI2, and GaMFI3.

To prepare mesoporous GaMFI zeolite, one gram of GaMFI2 zeolite was mixed with 10 mL of NaOH solution (0.2 M) at 70 °C for 2 h. After treatment, the zeolite was filtered and washed thoroughly with deionized water three times, and then dried at 110 °C overnight. Finally, the desilicated GaMFI2 zeolite was converted to H-form zeolites using the same procedure described above. The desilicated GaMFI2 zeolite was denoted as DS-GaMFI2.

3.3. Zeolite Characterizations

The composition of HZSM-5 zeolite and the Ga-containing MFI zeolites was determined by the X-ray fluorescence technique (XRF-1800, Shimadzu Co., Japan). XRD data of the zeolites were collected on a Bruker D8 Advanced powder X-RAY diffractometer using CuK α radiation.

The structural properties of the zeolites were obtained by N₂ phisical adsorption on a Micromeritics ASAP2020 Surface Area and Porosity Analyzer (Micromeritics Co., USA). Prior to the measurements, the zeolites were outgassed at 300 °C under vacuum for 12 h. The micropore volume was then calculated using *t*-plot method.

Pyridine-adsorbed Fourier Transform Infrared Spectroscopy analyses of the zeolites were conducted with Nicolet 5700 equipment (Thero Electron Co., USA). Zeolites were pressed into a regular wafer (10 mg, 13 mm diameter), and then treated at 400 °C in an IR cell for 2 h under vacuum.

The IR cell temperature was dropped to 100 °C, and then the background spectra were recorded. Pyridine was adsorbed on the samples, and followed by desorption at 200 °C. The concentrations of Lewis and Brønsted acid sites were then recorded on the basis of the intensity of 1450 cm⁻¹ (Lewis) and 1540 cm⁻¹ (Brønsted) bands.

Hydrogen-TPR experiments were carried on a chemisorption instrument (Autochem 2920, Micromeritics Co., USA). About 100 mg of the samples was pretreated at 550 °C for 1 h in helium stream, and then cooled down to 100 °C. The reduction was conducted in a mixture (H₂/Ar = 1/9) between 100 °C and 1000 °C with a ramp rate of 15 °C/min. The consumption of hydrogen was monitored by a TCD spectrometer.

3.4. Catalytic Fast Pyrolysis

CFP experiments were conducted on the Pyroprobe 5200 microreactor (CDS Analytical Co., USA). In brief, the zeolites were thoroughly mixed with beech wood powder in a zeolite-to-reactant ratio of 15. Approximately 4.5 mg of the mixtures were then fast pyrolyzed in the microreactor using a protocol described elsewhere [14,49]. The samples were rapidly heated to a present temperature (550 °C) with a ramp rate of 20 °C/ms, and then held for a minute under He flux. The final products generated via fast pyrolysis were carried by helium through a heated tube (300 °C) to GC (7890A, Agilent Co., USA) that was equipped with a flame ionization detector (FID), a thermal conductivity detector (TCD), and a mass spectrometer (5975C MSD). The gaseous products were conducted with an HP-Plot/Q column. The yields of hydrocarbons (aromatics, alkanes, and olefins) and carbon oxides (CO₂ and CO) were quantified with GC equipment, respectively. Triplicate experiments were conducted for the final product analyses, respectively. The carbon contents (char/coke) in the spent samples were measured by the elemental analyzer to determine the solid carbon yield. All yields are reported in terms of carbon yield according to Equation (1). The selectivity for aromatic hydrocarbons and xylene are calculated according to Equations (2) and (3), respectively.

$$\text{Carbon yield} = \frac{\text{Moles of carbon in a product}}{\text{Moles of carbon in reactant}} \times 100\% \quad (1)$$

$$\text{Aromatic selectivity} = \frac{\text{Moles of carbon in an aromatic product}}{\text{Moles of carbon in all aromatic products}} \times 100\% \quad (2)$$

$$\text{Xylene selectivity} = \frac{\text{Moles of a xylene isomer}}{\text{Moles of all xylene isomer}} \times 100\% \quad (3)$$

4. Conclusions

Hydrothermally synthesized Ga-MFI holds promise as a suitable catalyst for optimizing the distribution of aromatic products from CFP of biomass. Because of the deposition of non-framework Ga-oxides in their channels during calcination, Ga-MFI zeolites had a slightly narrowed effective micropore size relative to conventional HZSM-5, thus favoring the production of relative smaller aromatics such as benzene, toluene, and *p*-xylene over bulkier ones such as *m*-xylene, *o*-xylene, and polyaromatics. Consequently, Ga-MFI zeolites considerably enhanced the yield and selectivity of valuable monoaromatic product, especially *p*-xylene, and decreased the yield and selectivity of polyaromatics compared to conventional ZSM-5 zeolites during CFP of beech wood. The creation of intraparticle mesopores in Ga-MFI zeolites by desilication increased the overall yield of monoaromatics, mainly by increasing the production of *m*- and *o*-xylene, but decreased the yield and selectivity for *p*-xylene. These results indicate that carefully tuning the porosity of GaMFI zeolites may provide a feasible way to optimize the product distribution in CFP of biomass.

Author Contributions: J.L. conceived and designed the experiments; J.L., X.L. (Xiangyu Li), D.H., and X.L. (Xinning Lu) performed the experiments; J.L., X.L. (Xiangyu Li), and D.H. analyzed the data; J.L., X.L. (Xiangyu Li), and Y.W. wrote the paper.

Funding: This research was supported by the National Natural Science Foundation of China (Grant No. 21566001, No. 21606060 and No. 21663003).

Conflicts of Interest: The authors declared no conflict of interest.

References

1. Taarning, E.; Osmundsen, C.M.; Yang, X.; Voss, B.; Andersen, S.I.; Christensen, C.H. Zeolite-catalyzed biomass conversion to fuels and chemicals. *Energy Environ. Sci.* **2011**, *4*, 793–804. [[CrossRef](#)]
2. Gallezot, P. Conversion of biomass to selected chemical products. *Chem. Soc. Rev.* **2012**, *41*, 1538–1558. [[CrossRef](#)] [[PubMed](#)]
3. Huber, G.W.; Iborra, S.; Corma, A. Synthesis of transportation fuels from biomass: Chemistry, catalysts, and engineering. *Chem. Rev.* **2006**, *106*, 4044–4098. [[CrossRef](#)] [[PubMed](#)]
4. Zhang, X.S.; Lei, H.W.; Chen, S.L.; Wu, J. Catalytic co-pyrolysis of lignocellulosic biomass with polymers: A critical review. *Green Chem.* **2016**, *18*, 4145–4169. [[CrossRef](#)]
5. Zhang, L.; Bao, Z.; Xia, S.; Lu, Q.; Walters, K. Catalytic Pyrolysis of Biomass and Polymer Wastes. *Catalysts* **2018**, *8*, 659. [[CrossRef](#)]
6. Aho, A.; Kumar, N.; Eranen, K.; Salmi, T.; Hupa, M.; Murzin, D.Y. Catalytic pyrolysis of woody biomass in a fluidized bed reactor: Influence of the zeolite structure. *Fuel* **2008**, *87*, 2493–2501. [[CrossRef](#)]
7. Mihalcik, D.J.; Mullen, C.A.; Boateng, A.A. Screening acidic zeolites for catalytic fast pyrolysis of biomass and its components. *J. Anal. Appl. Pyrolysis* **2011**, *92*, 224–232. [[CrossRef](#)]
8. Jae, J.; Tompsett, G.A.; Foster, A.J.; Hammond, K.D.; Auerbach, S.M.; Lobo, R.F.; Huber, G.W. Investigation into the shape selectivity of zeolite catalysts for biomass conversion. *J. Catal.* **2011**, *279*, 257–268. [[CrossRef](#)]
9. Alejandro Martín, S.; Cerda-Barrera, C.; Montecinos, A. Catalytic Pyrolysis of Chilean Oak: Influence of Brønsted Acid Sites of Chilean Natural Zeolite. *Catalysts* **2017**, *7*, 356. [[CrossRef](#)]
10. French, R.; Czernik, S. Catalytic pyrolysis of biomass for biofuels production. *Fuel Process. Technol.* **2010**, *91*, 25–32. [[CrossRef](#)]
11. Yu, Y.; Li, X.; Su, L.; Zhang, Y.; Wang, Y.; Zhang, H. The role of shape selectivity in catalytic fast pyrolysis of lignin with zeolite catalysts. *Appl. Catal. A* **2012**, *447–448*, 115–123. [[CrossRef](#)]
12. Foster, A.J.; Jae, J.; Cheng, Y.T.; Huber, G.W.; Lobo, R.F. Optimizing the aromatic yield and distribution from catalytic fast pyrolysis of biomass over ZSM-5. *Appl. Catal. A* **2012**, *423*, 154–161. [[CrossRef](#)]
13. Carlson, T.R.; Jae, J.; Lin, Y.C.; Tompsett, G.A.; Huber, G.W. Catalytic fast pyrolysis of glucose with HZSM-5: The combined homogeneous and heterogeneous reactions. *J. Catal.* **2010**, *270*, 110–124. [[CrossRef](#)]
14. Yu, Y.; Zeng, Y.; Zuo, J.; Ma, F.; Yang, X.; Zhang, X.; Wang, Y. Improving the conversion of biomass in catalytic fast pyrolysis via white-rot fungal pretreatment. *Bioresour. Technol.* **2013**, *134*, 198–203. [[CrossRef](#)] [[PubMed](#)]
15. Thangalazhy-Gopakumar, S.; Adhikari, S.; Gupta, R.B.; Tu, M.; Taylor, S. Production of hydrocarbon fuels from biomass using catalytic pyrolysis under helium and hydrogen environments. *Bioresour. Technol.* **2011**, *102*, 6742–6749. [[CrossRef](#)] [[PubMed](#)]
16. Li, J.; Yu, Y.; Li, X.; Wang, W.; Yu, G.; Deng, S.; Huang, J.; Wang, B.; Wang, Y. Maximizing carbon efficiency of petrochemical production from catalytic co-pyrolysis of biomass and plastics using gallium-containing MFI zeolites. *Appl. Catal. B Environ.* **2015**, *172–173*, 154–164. [[CrossRef](#)]
17. Cheng, Y.T.; Wang, Z.; Gilbert, C.J.; Fan, W.; Huber, G.W. Production of p-xylene from biomass by catalytic fast pyrolysis using ZSM-5 catalysts with reduced pore openings. *Angew. Chem.* **2012**, *51*, 11097–11100. [[CrossRef](#)]
18. Li, J.; Li, X.Y.; Zhou, G.Q.; Wang, W.; Wang, C.W.; Komarneni, S.; Wang, Y.J. Catalytic fast pyrolysis of biomass with mesoporous ZSM-5 zeolites prepared by desilication with NaOH solutions. *Appl. Catal. A* **2014**, *470*, 115–122. [[CrossRef](#)]
19. Mei, C.; Wen, P.; Liu, Z.; Liu, H.; Wang, Y.; Yang, W.; Xie, Z.; Hua, W.; Gao, Z. Selective production of propylene from methanol: Mesoporosity development in high silica HZSM-5. *J. Catal.* **2008**, *258*, 243–249. [[CrossRef](#)]
20. Khan, W.; Jia, X.; Wu, Z.; Choi, J.; Yip, A. Incorporating Hierarchy into Conventional Zeolites for Catalytic Biomass Conversions: A Review. *Catalysts* **2019**, *9*, 127–149. [[CrossRef](#)]
21. Mochizuki, H.; Yokoi, T.; Imai, H.; Namba, S.; Kondo, J.N.; Tatsumi, T. Effect of desilication of H-ZSM-5 by alkali treatment on catalytic performance in hexane cracking. *Appl. Catal. A* **2012**, *449*, 188–197. [[CrossRef](#)]

22. Lai, P.C.; Chen, C.H.; Hsu, H.Y.; Lee, C.H.; Lin, Y.C. Methanol aromatization over Ga-doped desilicated HZSM-5. *RSC Adv.* **2016**, *6*, 67361–67371. [[CrossRef](#)]
23. Sadowska, K.; Góra-Marek, K.; Drozdek, M.; Kuśtrowski, P.; Datka, J.; Martinez Triguero, J.; Rey, F. Desilication of highly siliceous zeolite ZSM-5 with NaOH and NaOH/tetrabutylamine hydroxide. *Microporous Mesoporous Mater.* **2013**, *168*, 195–205. [[CrossRef](#)]
24. Vicente, J.; Gayubo, A.G.; Ereña, J.; Aguayo, A.T.; Olazar, M.; Bilbao, J. Improving the DME steam reforming catalyst by alkaline treatment of the HZSM-5 zeolite. *Appl. Catal. B Environ.* **2013**, *130–131*, 73–83. [[CrossRef](#)]
25. McGlone, J.; Priece, P.; Da Vià, L.; Majdal, L.; Lopez-Sanchez, J. Desilicated ZSM-5 Zeolites for the Production of Renewable p-Xylene via Diels–Alder Cycloaddition of Dimethylfuran and Ethylene. *Catalysts* **2018**, *8*, 253. [[CrossRef](#)]
26. Al-Yassir, N.; Akhtar, M.N.; Al-Khattaf, S. Physicochemical properties and catalytic performance of galloaluminosilicate in aromatization of lower alkanes: A comparative study with Ga/HZSM-5. *J. Porous Mater.* **2011**, *19*, 943–960. [[CrossRef](#)]
27. Fricke, R.; Kosslick, H.; Lischke, G.; Richter, M. Incorporation of Gallium into Zeolites: Syntheses, Properties and Catalytic Application. *Chem. Rev.* **2010**, *100*, 2303–2405. [[CrossRef](#)]
28. Marcilla, A.; Beltrán, M.I.; Navarro, R. Thermal and catalytic pyrolysis of polyethylene over HZSM5 and HUSY zeolites in a batch reactor under dynamic conditions. *Appl. Catal. B Environ.* **2009**, *86*, 78–86. [[CrossRef](#)]
29. Wang, K.; Kim, K.H.; Brown, R.C. Catalytic pyrolysis of individual components of lignocellulosic biomass. *Green Chem.* **2014**, *16*, 727–735. [[CrossRef](#)]
30. Ausavasukhi, A.; Huang, Y.; To, A.T.; Sooknoi, T.; Resasco, D.E. Hydrodeoxygenation of m-cresol over gallium-modified beta zeolite catalysts. *J. Catal.* **2012**, *290*, 90–100. [[CrossRef](#)]
31. Kim, J.W.; Park, S.H.; Jung, J.; Jeon, J.K.; Ko, C.H.; Jeong, K.E.; Park, Y.K. Catalytic pyrolysis of mandarin residue from the mandarin juice processing industry. *Bioresour. Technol.* **2013**, *136*, 431–436. [[CrossRef](#)] [[PubMed](#)]
32. Choudhary, V.R.; Kinage, A.K.; Sivadarayana, C.; Devadas, P.; Sansare, S.D.; Guisnet, M. H-gallosilicate (MFI) propane aromatization catalyst: Influence of Si/Ga ratio on acidity, activity and deactivation due to coking. *J. Catal.* **1996**, *158*, 34–50. [[CrossRef](#)]
33. Bjørgen, M.; Joensen, F.; Spangsborg Holm, M.; Olsbye, U.; Lillerud, K.P.; Svelle, S. Methanol to gasoline over zeolite H-ZSM-5: Improved catalyst performance by treatment with NaOH. *Appl. Catal. A* **2008**, *345*, 43–50. [[CrossRef](#)]
34. Holm, M.S.; Svelle, S.; Joensen, F.; Beato, P.; Christensen, C.H.; Bordiga, S.; Bjørgen, M. Assessing the acid properties of desilicated ZSM-5 by FTIR using CO and 2,4,6-trimethylpyridine (collidine) as molecular probes. *Appl. Catal. A* **2009**, *356*, 23–30. [[CrossRef](#)]
35. Al-Yassir, N.; Akhtar, M.N.; Ogunronbi, K.; Al-Khattaf, S. Synthesis of stable H-galloaluminosilicate MFI with hierarchical pore architecture by surfactant-mediated base hydrolysis, and their application in propane aromatization. *J. Mol. Catal. A Chem.* **2012**, *360*, 1–15. [[CrossRef](#)]
36. Ausavasukhi, A.; Sooknoi, T.; Resasco, D.E. Catalytic deoxygenation of benzaldehyde over gallium-modified ZSM-5 zeolite. *J. Catal.* **2009**, *268*, 68–78. [[CrossRef](#)]
37. Nowak, I. Effect of H₂–O₂ pre-treatments on the state of gallium in Ga/H-ZSM-5 propane aromatisation catalysts. *Appl. Catal. A* **2003**, *251*, 107–120. [[CrossRef](#)]
38. Gayubo, A.G.; Aguayo, A.T.; Atutxa, A.; Aguado, R.; Bilbao, J. Transformation of oxygenate components of biomass pyrolysis oil on a HZSM-5 zeolite. I. Alcohols and phenols. *Ind. Eng. Chem. Rev.* **2004**, *43*, 2610–2618. [[CrossRef](#)]
39. Gayubo, A.G.; Aguayo, A.T.; Atutxa, A.; Aguado, R.; Olazar, M.; Bilbao, J. Transformation of oxygenate components of biomass pyrolysis oil on a HZSM-5 zeolite. H. Aldehydes, ketones, and acids. *Ind. Eng. Chem. Rev.* **2004**, *43*, 2619–2626. [[CrossRef](#)]
40. Dorado, C.; Mullen, C.A.; Boateng, A.A. Origin of carbon in aromatic and olefin products derived from HZSM-5 catalyzed co-pyrolysis of cellulose and plastics via isotopic labeling. *Appl. Catal. B Environ.* **2015**, *162*, 338–345. [[CrossRef](#)]
41. Pérez-Ramírez, J.; Abelló, S.; Bonilla, A.; Groen, J.C. Tailored Mesoporosity Development in Zeolite Crystals by Partial Detemplation and Desilication. *Adv. Funct. Mater.* **2009**, *19*, 164–172. [[CrossRef](#)]

42. Zhu, X.; Lobban, L.L.; Mallinson, R.G.; Resasco, D.E. Tailoring the mesopore structure of HZSM-5 to control product distribution in the conversion of propanal. *J. Catal.* **2010**, *271*, 88–98. [[CrossRef](#)]
43. Choudhary, V.R.; Panjala, D.; Banerjee, S. Aromatization of propene and n-butene over H-galloaluminosilicate (ZSM-5 type) zeolite. *Appl. Catal. A* **2002**, *231*, 243–251. [[CrossRef](#)]
44. Choudhary, V.R.; Nayak, V.S.; Choudhary, T.V. Single-Component Sorption/Diffusion of Cyclic Compounds from Their Bulk Liquid Phase in H-ZSM-5 Zeolite. *Ind. Eng. Chem. Rev.* **1997**, *36*, 1812–1818. [[CrossRef](#)]
45. Park, H.J.; Heo, H.S.; Jeon, J.K.; Kim, J.; Ryoo, R.; Jeong, K.E.; Park, Y.K. Highly valuable chemicals production from catalytic upgrading of radiata pine sawdust-derived pyrolytic vapors over mesoporous MFI zeolites. *Appl. Catal. B Environ.* **2010**, *95*, 365–373. [[CrossRef](#)]
46. Cheng, Y.T.; Jae, J.; Shi, J.; Fan, W.; Huber, G.W. Production of renewable aromatic compounds by catalytic fast pyrolysis of lignocellulosic biomass with bifunctional Ga/ZSM-5 catalysts. *Angew. Chem.* **2012**, *51*, 1387–1390. [[CrossRef](#)] [[PubMed](#)]
47. Kim, Y.H.; Lee, K.H.; Nam, C.M.; Lee, J.S. Formation of Hierarchical Pore Structures in Zn/ZSM-5 to Improve the Catalyst Stability in the Aromatization of Branched Olefins. *ChemCatChem* **2012**, *4*, 1143–1153. [[CrossRef](#)]
48. Ohayon, D.; Le van Mao, R.; Ciaravino, D.; Hazel, H.; Cochenne, A.; Rolland, N. Methods for pore size engineering in ZSM-5 zeolite. *Appl. Catal. A* **2001**, *217*, 241–251. [[CrossRef](#)]
49. Torri, C.; Reinikainen, M.; Lindfors, C.; Fabbri, D.; Oasmaa, A.; Kuoppala, E. Investigation on catalytic pyrolysis of pine sawdust: Catalyst screening by Py-GC-MIP-AED. *J. Anal. Appl. Pyrolysis* **2010**, *88*, 7–13. [[CrossRef](#)]



© 2019 by the authors. Licensee MDPI, Basel, Switzerland. This article is an open access article distributed under the terms and conditions of the Creative Commons Attribution (CC BY) license (<http://creativecommons.org/licenses/by/4.0/>).